

PIMMS: Pulsation-Informed Magnetic Mapping of Stars with Zeeman-Doppler imaging

I. Formalism and numerical tests

C. Gutteridge^{1,*}, C. Neiner¹, C. Catala¹, and C. P. Folsom²

¹ LIRA, Observatoire de Paris, PSL University, CNRS, Sorbonne Université, Université Paris Cité, CY Cergy University, 5 place Jules Janssen, 92195 Meudon, France

² Tartu Observatory, University of Tartu, Observatooriumi 1, Tõravere 61602, Estonia

Received 10 June 2025 / Accepted 6 October 2026

ABSTRACT

Context. Magneto-asteroseismology is a novel technique allowing for more precise determinations of internal properties of magnetic pulsating stars, but it requires an accurate characterisation of the surface magnetic field that was not previously possible with Zeeman-Doppler imaging (ZDI) due to the time-dependent surface velocity of pulsating stars.

Aims. We aim to develop a new version of ZDI, which creates an additional surface velocity map that includes the time-dependent velocities of surface elements due to pulsations.

Methods. We present a new code, Pulsation-Informed Magnetic Mapping of Stars (PIMMS), which uses a surface-integrated line profile model that accounts for the additional Doppler shifts of local lines caused by pulsations. It is thus possible to fit this model to spectropolarimetric observations, reconstructing maps of the surface brightness, magnetic field, and the velocity field due to the combination of pulsation and rotation. In this paper, we present and explain how we tested PIMMS extensively, to understand its limitations and data requirements.

Results. We find that PIMMS can accurately reproduce the magnetic fields and brightness distributions of realistic models of pulsating hot stars. The required number of observations is higher than that required for ZDI of a non-pulsating star due to the additional velocity map that must be disentangled from surface brightness variations. PIMMS is now ready to be applied to real stars.

Key words. asteroseismology – line: profiles – methods: numerical – stars: magnetic field – stars: oscillations

1. Introduction

Zeeman-Doppler imaging (ZDI; Semel 1989) is a tomographic technique used to map the magnetic fields of stars using spectropolarimetric data. The Doppler shifts of stellar lines are dependent on the surface velocity, which is in turn dependent on the latitude of the source relative to the rotation axis, so they can therefore be used to probe positions. The Zeeman effect reveals the magnitude of the surface magnetic field strength at these positions through the size of the frequency separation of the split stellar lines, and orientation of the magnetic field through polarisation. ZDI is often performed with circularly polarised data (Stokes V) as the Zeeman signature in V is ~ 10 times stronger than in linearly polarised data (Stokes Q and U) for most stars. At the cost of extra observation time, ZDI can be performed with all Stokes parameters, which provides stronger constraints on the magnetic field and removes degeneracies in some cases (Kochukhov et al. 2004).

Many codes exist to reconstruct stellar magnetic fields, from the original work of Brown et al. (1991), built upon by Donati & Brown (1997), to INVERS13 (Kochukhov et al. 2013), and more recently ZDIPY (Folsom et al. 2018). All of these codes work on three assumptions: the star can be modelled as a sphere, the velocity at any point on the stellar surface is only dependent on position, and the only variation in observed magnetic field

strength and surface brightness is due to rotation. Hence, subsequent work has focussed on developing codes to account for stars for which these assumptions do not apply: the modification of ZDIPY by Cang et al. (2020) allows for the oblate geometries of rapid rotators, while the TIMES code (Finociety & Donati 2022) can map magnetic fields that vary on timescales less than the observing period. An attempt has previously been made to allow for ZDI of stars with an intrinsic variability in their surface brightness by Yu et al. (2017), using a simple model of linear variations in logarithmic relative surface brightness with time. This, however, was found only to provide minor improvements on standard ZDI as it could not fully represent the observed variability in surface features.

Zeeman-Doppler imaging has not been reliably performed for pulsating stars previously, as the stellar surface velocity is not solely dependent on rotation: a key assumption of all previous codes. Pulsating stars show variations in their line profiles due to the Doppler shifts caused by pulsation velocities (Fig. 1). In this paper we present the first ZDI code developed in order to account for the time-dependent surface velocity of pulsating stars: Pulsation-Informed Magnetic Mapping of Stars (PIMMS). Being able to accurately reconstruct magnetic field strengths and geometries from spectropolarimetric data will lead to more progress in the emerging field of magneto-asteroseismology, where asteroseismology is performed with the additional consideration of the surface and interior magnetic fields (Fuller et al. 2015; Li et al. 2022; Neiner 2024). Magnetic fields modify the

* Corresponding author: chloe.gutteridge@obspm.fr

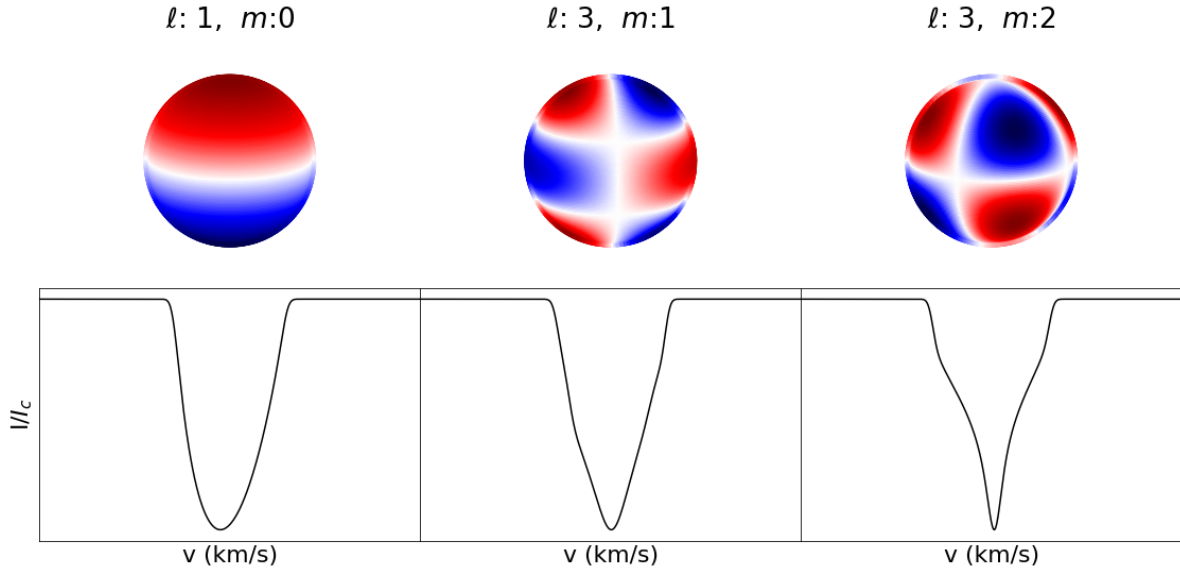


Fig. 1. Examples of line profiles for stars with three different pulsation modes, all with inclination angles of 75° .

pulsation modes and play an important role in the dynamics of the stellar interior, for instance by decreasing or suppressing internal differential rotation. These effects can be inferred if a surface magnetic field is detected and then taken into account in the modelling.

Due to a lack of targets with both sufficient spectropolarimetric data in addition to rich and well-defined pulsations, magneto-asteroseismology has so far been attempted for only three hot stars: the two β Cep stars β Cep itself (Shibahashi & Aerts 2000) and V2052 Oph (Briquet et al. 2012), and the SPB star HD 43317 (Buyschaert et al. 2018; Lecoanet et al. 2022). In the case of β Cep, the wrong rotation period was used in the model resulting in inaccurate results (Donati et al. 2001), while for V2052 Oph the magnetic field was only used to explain the seismic results rather than being included in the model itself. Only the model for HD 43317 is relatively complete, but for all three stars the magnetic field strength and geometry was determined without the precision that ZDI can provide.

In Sect. 2 we describe the stellar pulsation model and subsequent line profile synthesis we have implemented into ZDIPY to create PIMMS. We then explain how we extensively tested PIMMS in Sect. 3 with models of realistic hot magnetic pulsators. In Sect. 4, we examine factors that must be considered when applying PIMMS to real stars, then we discuss our results and conclusions in Sect. 5.

2. Stellar pulsation model

2.1. Initialisation file

Similar to ZDIPY, PIMMS requires certain variables to be assigned values prior to running, in an initialisation file. These include: the stellar parameters inclination i , limb darkening coefficient η , projected equatorial velocity $v_{\text{eq}} \sin i$, and rotation period, $P = 2\pi/\Omega$; the pulsation parameters degree ℓ , azimuthal order m , and frequency f ; and the model parameters resolution (number of surface elements), velocity range of the line profiles to be considered when fitting, and the Julian date for the start of rotation cycle 0. The file names are also provided here, alongside their Julian dates of observation, and central velocity corrections for line profiles due to barycentric and binary motion if present.

This is important as PIMMS only considers velocity variations due to pulsation, and would therefore try to fit these external velocity variations as such.

This file is also where fitting parameters can be controlled. PIMMS uses the maximum entropy image reconstruction algorithm from ZDIPY. Target values can be provided for both the C_{aim} and ‘TEST’ criteria (Skilling & Bryan 1984). C_{aim} controls the balance between maximum entropy and χ^2 in the final solution, while ‘TEST’ provides the convergence criterion of the model. Each map (pulsation or velocity, brightness, and magnetic) can be fitted individually or in any combination with one another, and those maps can then be loaded as constants or starting points for subsequent fits, which significantly improves the goodness of fit. For ZDIPY, which assumes a surface velocity constant in time, the suggested running order is to initially do a fit of the brightness map, then use that brightness map to fit the magnetic field map, then use both maps as a starting point for a final fit, where both are allowed to vary. For PIMMS, which additionally fits a time-dependent velocity map with pulsations, we suggest the following running order:

1. Fit only the pulsations (assuming a surface brightness uniform in space and time).
2. Using the fitted pulsation parameters, fit the surface brightness.
3. Fit both pulsation and brightness, using the results from the previous two fits as initial parameters.
4. Keep the pulsation parameters and surface brightness map from the previous fit constant while fitting the magnetic field.
5. Use the results of the previous fit as the starting point for a final fit that allows all pulsation, brightness, and magnetic field parameters to vary.

The allowed field geometries can also be controlled. PIMMS uses the exact same spherical harmonic description of the magnetic field and fitting methods as in ZDIPY, which follow Donati et al. (2006). The constants $\alpha_{\ell m}$, $\beta_{\ell m}$, and $\gamma_{\ell m}$ describe the contributions of the radial field, the azimuthal and meridional terms of the poloidal field, and the azimuthal and meridional terms of the toroidal field respectively, for each spherical harmonic component of degree ℓ and order m . Fitting only certain constants or constraining the allowed values will result in different field structures: fitting α and β , and setting $\gamma = 0$ provides a poloidal

field; fitting $\alpha = \beta$, and setting $\gamma = 0$ provides a potential field; fitting $\alpha = \beta$ and γ provides a potential-toroidal field. Fitting all three unconstrained allows for an arbitrary vector field. The complexity of the allowed magnetic field is controlled by the number of spherical harmonic components fitted. For a maximal spherical harmonic degree ℓ_{\max} , there are $N_{\text{sph}} = \frac{1}{2}\ell_{\max}(\ell_{\max} + 3)$ components. ℓ_{\max} is provided in the initialisation file and should be carefully set when performing ZDI with either ZDIPY or PIMMS to ensure sufficient complexity to accurately describe the field.

2.2. Stellar surface grid

We began by defining a unit sphere, on a system of Cartesian axes, that the stellar model will be described by. We have:

$$x = \sin \theta \cos \phi, \quad y = \sin \theta \sin \phi, \quad z = \cos \theta, \quad (1)$$

where polar angle θ is the angle from the Z axis to the radial line from the origin to a given point (x, y, z) , while the azimuthal angle ϕ is the angle between the X axis and projection of the point onto the $X - Y$ plane.

We then separated the unit sphere into surface area elements of approximately equal area A , calculated by Eq. (2). We did this first by separating the sphere into rings of equal latitude ranges, and calculating the surface area of each ring, $A_{\theta_1 \rightarrow \theta_2}$, using Eq. (3). We then allocated a number of elements proportional to the fraction of the total surface area each ring contains, equally spaced them in longitude, and calculated the true areas of each of these surface elements:

$$A = \iint \sin \theta \, d\theta \, d\phi, \quad (2)$$

$$A_{\theta_1 \rightarrow \theta_2} = 2\pi |\cos \theta_1 - \cos \theta_2|. \quad (3)$$

We first asserted that the rotation axis, which we chose to be the Z axis, is perpendicular to the line of sight to the star. We need to transform this model to account for the inclination angle of the star's rotation and pulsation axis to the line of sight. In PIMMS we assume these to be the same, as is the case in most stars. Notable exceptions include roAp stars (Kurtz 1982) and stars with tidally induced pulsations (Reed et al. 2005), the latter of which is non-spherical and therefore would not be well represented by our model regardless. The rotation matrix about the Cartesian axes can be defined as:

$$R = \begin{pmatrix} \cos(b) \cos(c) & \sin(a) \sin(b) \cos(c) & \cos(a) \sin(b) \cos(c) \\ & -\cos(a) \sin(c) & +\sin(a) \sin(c) \\ \cos(b) \sin(c) & \sin(a) \sin(b) \sin(c) & \cos(a) \sin(b) \sin(c) \\ & +\cos(a) \cos(c) & -\sin(a) \cos(c) \\ -\sin(b) & \sin(a) \cos(b) & \cos(a) \cos(b) \end{pmatrix}, \quad (4)$$

where a , b , and c are the angles about the X , Y , and Z axes respectively.

To rotate the model star, we applied a transformation using $c = \Omega t$, where Ω is the angular rotation frequency of the star and t is the time past since reference time 0, for example Eq. (5):

$$R_{\Omega} = \begin{pmatrix} \cos(\Omega t) & -\sin(\Omega t) & 0 \\ \sin(\Omega t) & \cos(\Omega t) & 0 \\ 0 & 0 & 1 \end{pmatrix}. \quad (5)$$

To incline the star, we set a to the inclination angle i provided in the initialisation file:

$$R_i = \begin{pmatrix} 1 & 0 & 0 \\ 0 & \cos(i) & -\sin(i) \\ 0 & \sin(i) & \cos(i) \end{pmatrix}. \quad (6)$$

2.3. Stokes profiles

We followed the derivation of Eq. (6.49) in Aerts et al. (2010) to describe the observed line profile. The line forming region was assumed to be geometrically thin, so that the dependence of velocity and magnetism on line depth can be ignored. Each local line profile p_{ij} , for surface element (i, j) , can be approximated as a normalised Gaussian. i and j are the indexes in colatitude θ and longitude ϕ respectively. The variance, σ , controls the intrinsic line width, which is affected by natural, pressure, and thermal broadening:

$$p_{ij}(v, t) = \frac{1}{\sqrt{2\pi}\sigma} \exp\left(-\frac{(v_{ij}(t) - v)^2}{2\sigma^2}\right). \quad (7)$$

Each local line was Doppler shifted by an amount dependent on the velocity of its corresponding area element, giving the new line centre on the velocity axis, v_{ij} . This velocity is dependent on both rotation and pulsation velocities, the latter of which is dependent on time, t . Eq. (9) defines the total velocity along the line of sight to the observer. θ'_i and ϕ'_j are the coordinates θ_i and ϕ_j transformed such that the polar axis is inclined by stellar inclination angle i , while the zero point of the azimuthal angles remains the same.

The pulsation velocities in the spherical coordinate system were defined as follows:

$$\begin{pmatrix} v_r \\ v_{\theta} \\ v_{\phi} \end{pmatrix}_{\text{puls}} = \begin{pmatrix} \Xi_{nl}(r) P_l^m(\cos \theta) \sin(m\phi - \omega t - \varphi) \\ \Theta_{nl}(r) \frac{dP_l^m(\cos \theta)}{d\theta} \sin(m\phi - \omega t - \varphi) \\ \Theta_{nl}(r) \frac{m}{\sin \theta} P_l^m(\cos \theta) \cos(m\phi - \omega t - \varphi) \end{pmatrix}_{\text{puls}} \quad (8)$$

and were transformed to Cartesian coordinates by matrix $S(\theta_i, \phi_j)$. The velocity along the line of sight is defined as $v_{z,ij}$:

$$\begin{pmatrix} v_{x,ij} \\ v_{y,ij} \\ v_{z,ij} \end{pmatrix}_{\text{puls}} = R_i R_{\Omega} S(\theta_i, \phi_j) \begin{pmatrix} v_{r,ij} \\ v_{\theta,ij} \\ v_{\phi,ij} \end{pmatrix}_{\text{puls}}, \quad (9)$$

where

$$S(\theta_i, \phi_j) = \begin{pmatrix} \sin \theta_i \cos \phi_j & \cos \theta_i \cos \phi_j & -\sin \phi_j \\ \sin \theta_i \sin \phi_j & \cos \theta_i \sin \phi_j & \cos \phi_j \\ \sin \theta_i \cos \phi_j & \cos \theta_i \cos \phi_j & 0 \end{pmatrix}. \quad (10)$$

The pulsation parameters degree $\ell \geq 0$, azimuthal order $m \in [-\ell, +\ell]$, and frequency f were provided for each pulsation mode, along with inclination angle i , and equatorial velocity v_{Ω} for the star. The following pulsation variables were fitted: tangential to radial displacement ratio K , pulsation velocity v_p , and phase φ at time $t = 0$ defined in the initialisation file. $P_{\ell}^m(\cos \theta)$ are Legendre functions given for $m \geq 0$ by

$$P_{\ell}^m(\cos \theta) = \frac{1}{2^{\ell} \ell!} (1 - \cos^2 \theta)^{m/2} \frac{d^{\ell+m}}{d \cos^{\ell+m} \theta} (\cos^2 \theta - 1)^{\ell}. \quad (11)$$

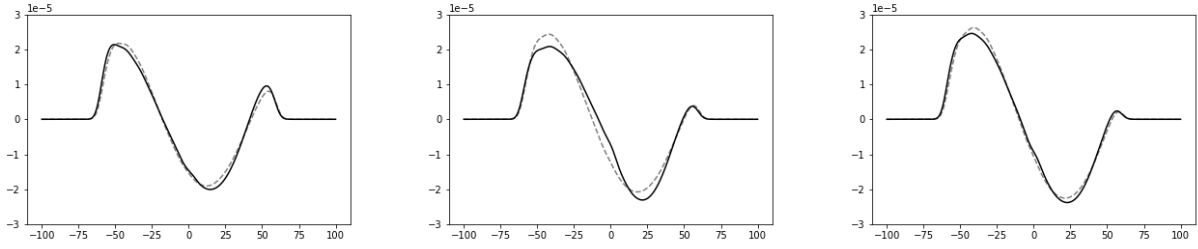


Fig. 2. Model Stokes V signatures for stars at rotation phases 0, 0.5, and 1. The solid black line is for a star with a single $\ell = 2$, $m = -2$ pulsation mode, while the dashed grey line is for a non-pulsating star. The stars have a uniform surface brightness, and identical rotation periods and magnetic fields. The model Stokes V signatures deviate strongly from each other, even at equivalent rotation phases i.e. 0 and 1, due to the pulsation velocities.

We removed the differential factor in the Legendre function, to provide an analytical solution for use in PIMMS, using the binomial theorem expansion, and the substitution $\vartheta = \cos \theta$:

$$\begin{aligned} P_\ell^m(\vartheta) &= \frac{1}{2^\ell \ell!} (1 - \vartheta^2)^{m/2} \frac{d^{\ell+m}}{d\vartheta^{\ell+m}} (\vartheta^2 - 1)^\ell \\ &= \frac{1}{2^\ell \ell!} (1 - \vartheta^2)^{m/2} \frac{d^{\ell+m}}{d\vartheta^{\ell+m}} \left[\sum_{k=0}^{\ell} (-1)^k \frac{\ell!}{k!(\ell-k)!} \vartheta^{2(\ell-k)} \right] \\ &= \frac{1}{2^\ell} (1 - \vartheta^2)^{m/2} \sum_{k=0}^{k \leq \frac{\ell-m}{2}} \frac{(-1)^k}{k!(\ell-k)!} \frac{[2(\ell-k)]!}{[\ell-2k-m]!} \vartheta^{\ell-2k-m}. \end{aligned} \quad (12)$$

Reversing the $\vartheta = \cos \theta$ substitution, and introducing a function $\kappa(\ell, m, k)$ dependent only on the mode parameters, we obtained the form used in the code to compute the Legendre functions:

$$P_\ell^m(\cos \theta) = \sin^m \theta \sum_{k=0}^{k \leq \frac{\ell-m}{2}} \kappa(\ell, m, k) \cos^{\ell-2k-m} \theta, \quad (13)$$

where $\kappa(\ell, m, k)$ is defined as

$$\kappa(\ell, m, k) = \frac{1}{2^\ell} \frac{(-1)^k}{k!(\ell-k)!} \frac{[2(\ell-k)]!}{[\ell-2k-m]!}. \quad (14)$$

We then need to differentiate Eq. (13) by θ for the differential term in the sum of Eq. (8):

$$\begin{aligned} \frac{dP_\ell^m(\cos \theta)}{d\theta} &= \frac{d \sin^m \theta}{d\theta} \sum_{k=0}^{k \leq \frac{\ell-m}{2}} \kappa(\ell, m, k) \cos^{\ell-2k-m} \theta \\ &\quad + \sin^m \theta \sum_{k=0}^{k \leq \frac{\ell-m}{2}} \kappa(\ell, m, k) \frac{d \cos^{\ell-2k-m} \theta}{d\theta} \\ &= \sin^{m-1} \theta \sum_{k=0}^{k \leq \frac{\ell-m}{2}} \kappa(\ell, m, k) \cos^{\ell-2k-m-1} \theta \\ &\quad \times [m + (2k - \ell) \sin^2 \theta]. \end{aligned} \quad (15)$$

For $m < 0$, a proportionality relationship can be used:

$$P_\ell^{-m}(\cos \theta) = (-1)^m \frac{(\ell - m)!}{(\ell + m)!} P_\ell^m(\cos \theta). \quad (16)$$

As Eq. (16) is linear, the constant factors can also be used to give the differentiated associate Legendre polynomials with $m < 0$, i.e.

$$\frac{dP_\ell^{-m}(\cos \theta)}{d\theta} = (-1)^m \frac{(\ell - m)!}{(\ell + m)!} \frac{dP_\ell^m(\cos \theta)}{d\theta}. \quad (17)$$

Each local line profile was weighted in the sum by the brightness of the elemental area associated. The weights were calculated from product of: the continuum intensity at (θ_i, ϕ_j) , I_0 ; the projected area of the element, $\sin \theta'_i \cos \theta'_i \Delta \theta'_i \Delta \phi'_j$; and the limb darkening coefficient $h_\lambda(\theta'_i)$, from the linear limb darkening law $h_\lambda(\theta'_i) = 1 - \eta + \eta \cos(\theta'_i)$ (Gray 2005). This is the same limb darkening law used in the ZDIPY. The sum was taken over the visible stellar surface, i.e. $\theta' \in [0, \frac{\pi}{2}]$, $\phi' \in [0, 2\pi]$, and renormalised by the sum of the weights. Eq. (18) is equivalent to the Stokes I profile:

$$p(v, t) = 1 - \frac{\sum_{i,j} I_0(\theta_i, \phi_j) h_\lambda(\theta'_i) p_{ij}(v, t) \sin \theta'_i \cos \theta'_i \Delta \theta'_i \Delta \phi'_j}{\sum_{i,j} I_0(\theta_i, \phi_j) h_\lambda(\theta'_i) \sin \theta'_i \cos \theta'_i \Delta \theta'_i \Delta \phi'_j}. \quad (18)$$

The magnetic model remains unchanged from ZDIPY, albeit with the Stokes V profiles now calculated from the derivative of the new line profile model:

$$V_{ij}(\lambda) = g_{\text{eff}} \frac{\lambda_0^2 e}{4\pi m_e c} B_{l,ij} \frac{dp_{ij}(v, t)}{dv} \frac{dv}{d\lambda}. \quad (19)$$

Examples of our model Stokes V profiles can be seen in Fig. 2. As the pulsations affect the Stokes V signature, the magnetic field model can inform our pulsation fit, which is why we recommend allowing all parameters to vary in the final step of running PIMMS.

3. Tests on simulations

For the following tests, we used PIMMS to generate the simulated line profiles, using approximately 10 000 equally sized cells to represent the stellar surface. The model was inclined in rotation by $i = 55^\circ$ and the magnetic field was inclined to the rotation axis by $\beta = 40^\circ$. The star rotates with a frequency of $f_{\text{rot}} = 1.10 \text{ d}^{-1}$, corresponding to $v \sin i = 60 \text{ km s}^{-1}$, and has a local line width of $\sigma = 3 \text{ km s}^{-1}$. We followed the ideal fitting order described in Sect. 2.1, and allowed fitting of magnetic field topologies up to spherical harmonic degree $\ell_{\text{max}} = 5$, though our test field is a simple dipole ($\ell_{\text{max}} = 1$). Our test pulsation mode parameters, representative of real pulsating stars, can be found in Table 1. These are the measured pulsation mode parameters of β Cep star V2052 Oph, from Briquet et al. (2012). We added Gaussian noise to every model line profile to give signal-to-noise ratios (S/N) of 1900, which replicate ideal but realistic observations.

Table 1. Pulsation mode parameters used to test PIMMS.

ID	f (d^{-1})	ℓ	m
f_1	7.14846	0	0
f_2	7.75603	4	3
f_3	6.82308	4	2

Notes. The pulsation modes used are taken from Briquet et al. (2012) for the magnetic β Cep star V2052 Oph.

Table 2. Summary of input and best-fit values for the ZDIPY and PIMMS codes, when applied to 100 simulated observations of a β Cep star with a dipolar magnetic field and uniform surface brightness, as described in Sect. 3.1.

Parameter	Input	ZDIPY	PIMMS
$v_{p,1}$	20.0000		20.0217
φ_1	0.0000		0.0005
K_1	0.0000		0.0000
$v_{p,2}$	0.5000		0.4958
φ_2	0.3000		0.3001
K_2	0.0100		0.0109
$v_{p,3}$	0.5000		0.5088
φ_3	0.7000		0.7093
K_3	0.1000		0.0754
B_d	583	523	581

Table 3. Summary of input and best-fit values for the ZDIPY and PIMMS codes, when applied to 100 simulated observations of a β Cep star with a dipolar magnetic field and a single spot on the magnetic pole, as described in Sect. 3.2.

Parameter	Input	ZDIPY	PIMMS
$v_{p,1}$	20.0000		20.0193
φ_1	0.0000		0.0005
K_1	0.0000		0.0004
$v_{p,2}$	0.5000		0.5074
φ_2	0.3000		0.3002
K_2	0.0100		0.0110
$v_{p,3}$	0.5000		0.5207
φ_3	0.7000		0.7088
K_3	0.1000		0.0971
B_d	583	514	594

3.1. Star with a dipolar magnetic field and a uniform surface brightness

We began by testing the ability to fit the pulsations of a star with a uniform surface brightness. We provided 100 observations equally spread over the rotation phase to ensure that the rotation phase coverage is not the limitation. The pulsation phase was well covered due to the comparatively short pulsation frequencies. ZDIPY failed to produce a physical brightness map, instead outputting a completely dark star with bright spots along a line of latitude around $+15^\circ$ (see middle panel of Fig. 3). This angle corresponds to $i - \beta$. ZDIPY produces this wrong brightness map because it tries to compensate for the pulsations with spots, but as the rotation and pulsation frequencies are not at all similar, the resulting fitted line profiles do not resemble the simulated observations. We tested the ability of ZDIPY to fit the magnetic field assuming a uniform surface brightness, but even when the

true surface brightness was provided, ZDIPY failed to reproduce the magnetic field, due to the incorrect attribution of velocities to position, resulting in additional weak poles being added (see middle panel of Fig. 4). This confirms that ZDIPY should not be used for pulsating stars.

PIMMS reproduces the uniform surface brightness correctly, with only very minor and evenly distributed variations due to the added noise (see right-hand panel of Fig. 3). The recovered magnetic field is essentially the same as the inputted field, with differences $<1\%$ (see right-hand panel of Fig. 4). Using the inputted uniform surface brightness instead of the fitted surface brightness causes no significant difference in the model magnetic field when tested with a perfect dipole. Parameters and results of this test are summarized in Table 2.

3.2. Star with a dipolar magnetic field and a spotted surface

We progressed to a pulsating star with a single spot, aligned with the visible pole of the dipolar magnetic field. We again provided 100 observations equally spread over the rotation phase to ensure that the phase coverage was not the limitation. When applying ZDIPY, it resulted in an entirely dark star, except at the pole and again the line of latitude around $+15^\circ$ which it considered bright (see middle panel of Fig. 5). Once again, even when the true surface brightness was provided, ZDIPY failed to reproduce the magnetic field, with field strength being incorrectly attributed to higher order polar terms (see middle panel of Fig. 6).

In contrast, PIMMS produces the inputted polar spot, albeit smoothed out (see right-hand panel of Fig. 5), because of the noise we added to the input data and the sampling of rotation phase. This smoothing causes slight overestimation of the field strength near the pole, but differences with regard to the inputted field are $<2\%$ (see right-hand panel of Fig. 6), and the position of the pole is not affected. This must nonetheless be taken seriously, as for the hot magnetic stars there are often temperature spots on the poles. The overestimation can be corrected by limiting the spherical harmonic degree ℓ_{\max} to a lower value, but in a real case where we do not know the true topology, we could be losing resolution in structure and incorrectly attributing to increased strength in spots. Parameters and results of this test are summarized in Table 3.

3.3. Required number of observations

The number of observations required to reliably constrain the magnetic and pulsation model is dependent on many variables, such as the number of pulsation modes, the mode geometries, number of chemical spots, magnetic field geometry, phase coverage distribution, and precision aim (see Sect. 4 for more detail). It is therefore not possible to give a simple value here. In cases where a preliminary characterisation of the stellar magnetic field exists, and the pulsation modes have been previously identified, we advise modelling the star with these expected pulsation modes and magnetic field geometry in advance of observing, in order to estimate how many additional data must be obtained. Here we demonstrate the data requirements for a model β Cep star based on V2052 Oph, and a model SPB star with a single pulsation frequency close to its rotation frequency. Our β Cep model has a dipolar field, spots on the magnetic poles (rather than the off-centre helium poles in the case of V2052 Oph), and the three pulsation modes given in Table 1. This β Cep model can be interpreted as the minimum data requirement for PIMMS to operate due to its relative simplicity. Our SPB model also has a dipolar field, with off-pole spots, and a single non-radial pulsation mode, ($\ell = 2$, $m = 0$, $f = 1.15 d^{-1}$). We

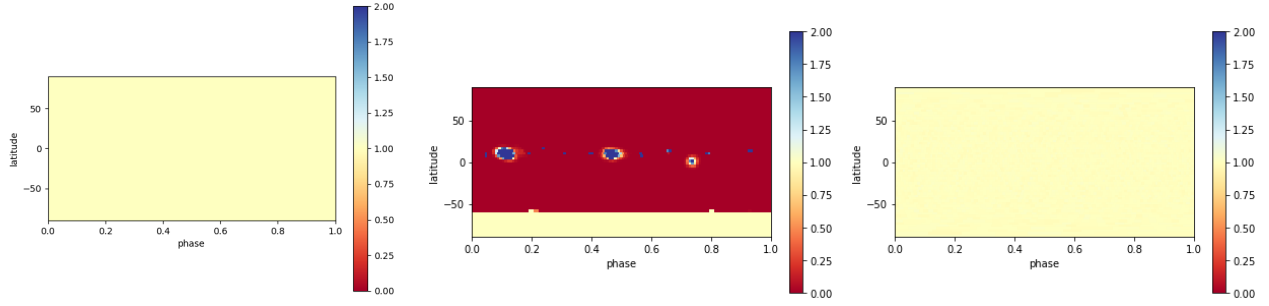


Fig. 3. Results of a test for a dipolar star with uniform brightness. The left-hand plot is the brightness map used to generate the model line profiles we test the codes on, the middle is the best-fit brightness map produced by ZDIPY, and the final plot is the best-fit brightness map produced by PIMMS.

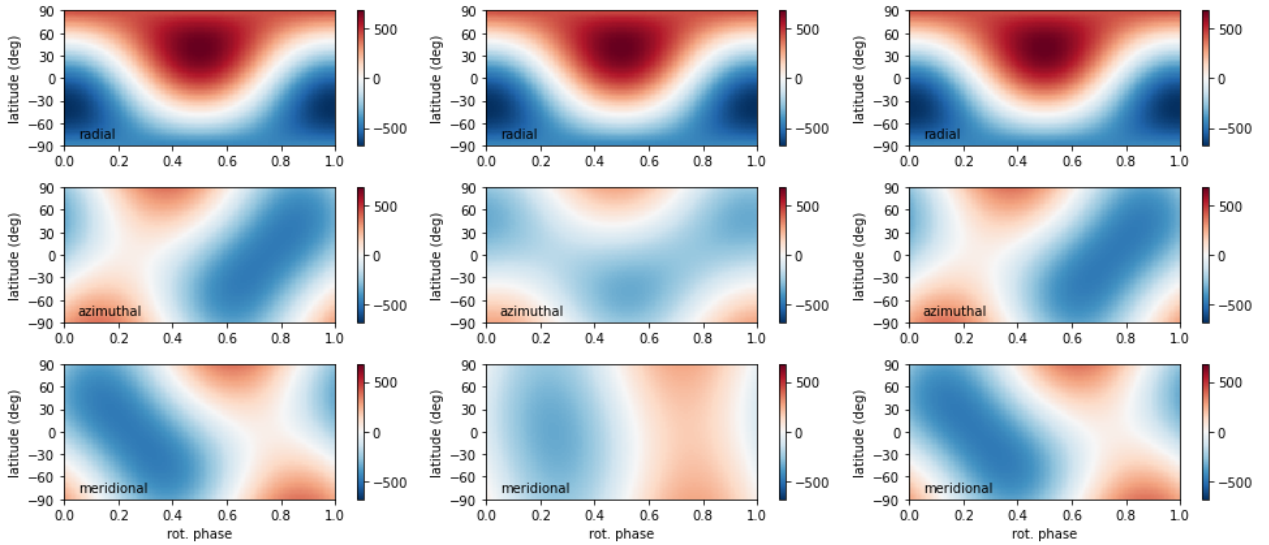


Fig. 4. Results of a test for a dipolar star with uniform brightness. The left-hand plot is the magnetic map used to generate the model line profiles we test the codes on, the middle is the outputted magnetic field map from ZDIPY assuming the input surface brightness map, and the final plot is the magnetic field map from PIMMS using the fitted brightness map.

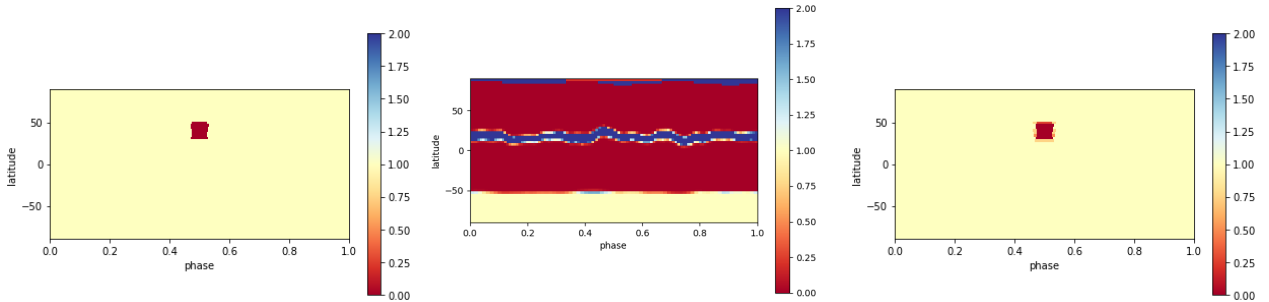


Fig. 5. Same as Fig. 3, but for a star with a singular polar spot.

set the rotation frequency to $f_{\text{rot}} = 1.10 \text{ d}^{-1}$ to demonstrate a much more complicated case where the pulsation must be disentangled from permanent features, i.e. spots. In both cases, we aimed for a fit threshold of $\chi^2 < 1.5$. See Table 4 for a summary of the parameters and results of these tests.

First, we considered the case where we are able to schedule our observations such that we can perfectly distribute them over a single rotation cycle. In this case, we recover the field strength and structure with a minimum of 19 observations for our model β Cep pulsator. It should however be noted that mode identification would be difficult with so few observations. In cases where the pulsation modes have been well studied in pure spectroscopy,

such that mode identification from spectropolarimetric observations is not required, equally spacing observations over the rotation phase could be an adequate observation strategy. However, the pulsation phase coverage must nonetheless still be considered, and strongly affects the goodness of fit. The required number of observations is significantly higher for our model SPB at 109. Although there is only a single pulsation mode present, it needs to be disentangled from the line profile variations caused by spots, which is difficult over a single rotation period when the frequencies are so close. Although it converges with an ideal χ^2 value, it does so with additional small surface brightness features not present in the input map. This suggests

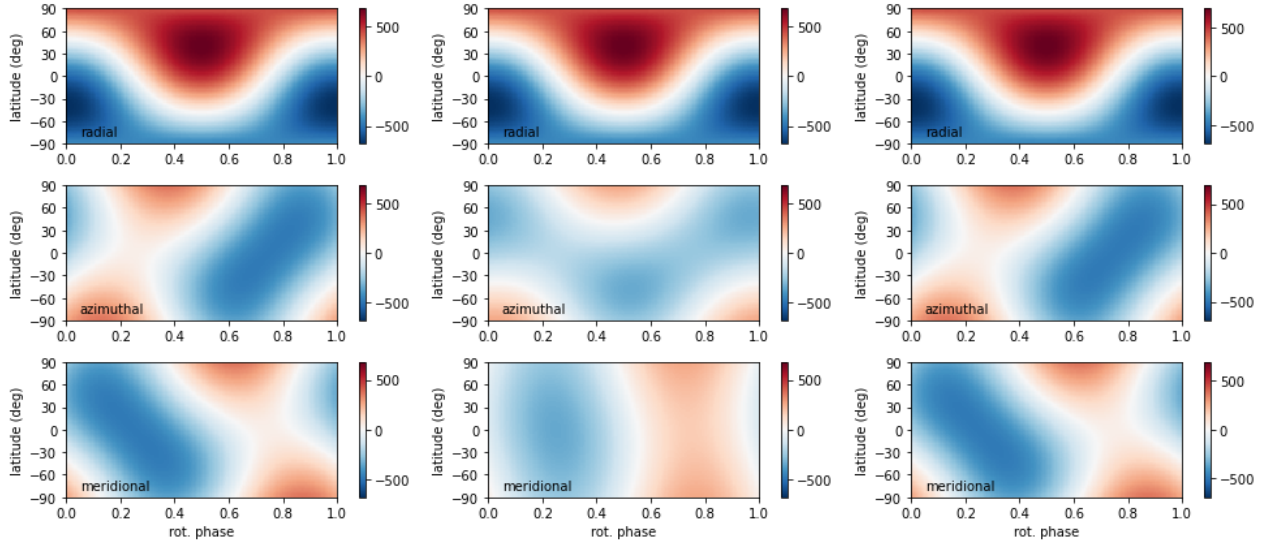


Fig. 6. Same as Fig. 4, but for a star with a singular polar spot.

Table 4. Summary of input and best-fit values for the PIMMS code when running on the minimum required number of observations, equally spread across a single rotation period, of the simulated β Cep and SPB stars described in Sect. 3.3.

Parameter	β Cep model		SPB model	
	Input	PIMMS	Input	PIMMS
$v_{p,1}$	20.0000	20.0194	15.0000	14.1673
φ_1	0.0000	0.0005	0.2000	0.2004
K_1	0.0000	0.0005	0.0100	0.0129
$v_{p,2}$	0.5000	0.5074		
φ_2	0.3000	0.3002		
K_2	0.0100	0.0110		
$v_{p,3}$	0.5000	0.5205		
φ_3	0.7000	0.7091		
K_3	0.1000	0.0926		
B_d	583	581	583	589

Notes. The number of observations is 19 and 109 for the β Cep and SPB models respectively. The β Cep star has 3 pulsation modes, and spots on the magnetic poles, while the SPB has a single pulsation mode and off-pole spots. Both models have dipolar magnetic fields.

that observations spanning multiple rotation cycles would be helpful.

Then we considered observations scheduled over 6 months (to reflect a telescope semester of observations) with the gaps in phase over both rotation and pulsation cycles minimised (see Table 5). For our model β Cep pulsator, this only slightly improves the minimum number of observations to 18. By improving the phase coverage in pulsation, a marginally better fit is obtained in the pulsation step with less data required. For our model SPB, the required number of observations is 52. Spreading the observations across multiple rotation cycles drives this reduction (see Sect. 4.5).

Finally we considered observations scheduled at random over 6 months, and repeated this test 100 times. This situation occurs when the stellar rotation period is not known before observations or when phase-constrained observations cannot be scheduled at the telescope. We find that the average minimum number of observations required to fit the model β Cep with $\chi^2 < 1.5$ is 24,

Table 5. Summary of input and best-fit values for the PIMMS code when running on the minimum required number of observations, where the gaps in rotation and pulsation phase were minimised, of the simulated β Cep and SPB stars described in Sect. 3.3.

Parameter	β Cep model		SPB model	
	Input	PIMMS	Input	PIMMS
$v_{p,1}$	20.0000	20.0194	15.0000	14.8760
φ_1	0.0000	0.0005	0.2000	0.2004
K_1	0.0000	0.0005	0.0100	0.0116
$v_{p,2}$	0.5000	0.5074		
φ_2	0.3000	0.3002		
K_2	0.0100	0.0110		
$v_{p,3}$	0.5000	0.5205		
φ_3	0.7000	0.7090		
K_3	0.1000	0.0950		
B_d	583	581	583	586

Notes. The number of observations is 18 and 52 for the β Cep and SPB models respectively. The β Cep star has 3 pulsation modes, and spots on the magnetic poles, while the SPB has a single pulsation mode and off-pole spots. Both models have dipolar magnetic fields.

while the model SPB is 68. As a general rule, gaps in rotation phase over 0.15, and in pulsation phase over 0.25, will not provide a well constrained magnetic map and pulsation parameters. We stress that these numbers are for simple examples with few low-order pulsation modes, and a dipolar field. More complex stars will require more observations, as discussed below.

4. Considerations for application to real stars

4.1. Limits of Zeeman-Doppler imaging as a technique

First, it is important to briefly discuss the limits of ZDI itself, such that the distinction can be made of whether deficiencies occur in just PIMMS or the technique as a whole. ZDI is a tomographic technique and hence is dependent on rotational modulation detectable in the observations. For stars with low $v_{\text{eq}} \sin i$ values, high resolution spectropolarimetry is necessary to be able to detect variations in the line profile. In the case of

stars that are pole-on, there is no modulation in the line profiles associated with rotation, and therefore it is impossible to perform ZDI, regardless of the code used. Likewise, for equator-on stars, there is a degeneracy between the northern and southern hemispheres which makes ZDI mapping inevitably inaccurate. In fact, with Stokes V inversion only there is an overall uniqueness problem with ZDI, well exemplified by the study of τ Sco by Kochukhov & Wade (2016). Multiple different magnetic field strengths and geometries produced indistinguishable Stokes V profiles for this star. It is also well established in ZDI that there is significant crosstalk between the radial to meridional magnetic fields at low latitudes (Donati & Brown 1997; Kochukhov & Piskunov 2002). While it is possible to largely solve the uniqueness problem by introducing Stokes Q and U observations, this is impractical for many stars due to the significantly higher S/N required for a magnetic detection in linear polarisation data. Regardless of the Stokes parameters used, fine scale structure will always be lost due to its sensitivity to noise and intrinsic line broadening, which provides a limit on the spatial scales that can be reconstructed.

It is necessary to use Stokes I data to reconstruct a map of surface weights to the measured magnetic field (e.g. Rosén & Kochukhov 2012). These can be in the form of brightness, temperature or abundance maps. Spots recovered in ZDI are often smeared due to the sampling of the data, as we found in Sect. 3.2. This has little effect on the recovered magnetic field if not subject to over-fitting.

4.2. Model resolution requirements

Care must be taken when selecting the number of surface elements used for the model star. While running with an unnecessarily high resolution does not produce negative outputted results, it does strongly affect the runtime. On the other hand, an insufficient resolution can significantly harm the results. Higher degree pulsation modes cause sharper changes in velocity, which cannot be well represented in a low resolution map. High velocities also cause an increase in the difference in Doppler shift between surface elements, so a greater spacial resolution is needed for stars with large pulsation velocities, or $v_{\text{eq}} \sin i$ values. Additionally, low resolution increases the level of smoothing in the brightness maps, therefore affecting strengths in the magnetic map. Correct selection of the resolution can be verified by looking at the outputted model line profiles, such as Fig. 7.

4.3. Signal-to-noise requirements

The tests shown in Sect. 3 used data with a signal-to-noise ratio (S/N) in the model line profile of 1900, but we have successfully mapped model stars with S/N down to 250. This would be sufficient to detect a strong magnetic field in a star with a low $v_{\text{eq}} \sin i$, such as the magnetic fields of B stars which have a median B_d value of 3 kG (Shultz et al. 2019). Added noise has more significant effects on fitting the brightness map than the magnetic field mapping individually, but when fitting both together the noise can create errors in field structure and strengths. Ultimately, the limiting factor for S/N is more likely to be in detecting the magnetic field in the first place, and pulsation mode identification if done with spectropolarimetric data.

4.4. Pulsation phase coverage

As briefly mentioned in Sect. 3.3, the phase coverage requirement for pulsation is less than that for rotation. Similar to all

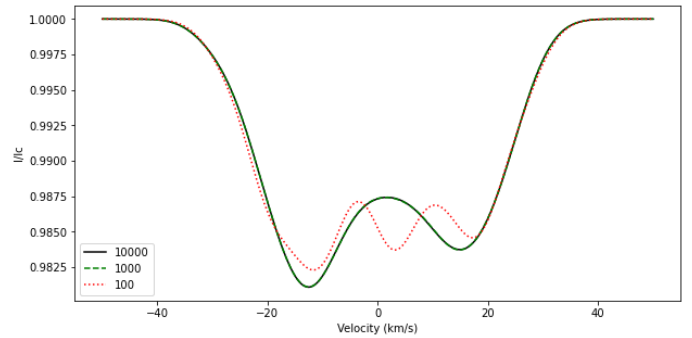


Fig. 7. Comparison between the line profiles of a $\ell = 5$, $m = -5$ mode generated for three different resolutions. The solid black line is the higher resolution model using 10 000 equally sized cells on the stellar surface, while the green dashed line is the 1000 cell moderate resolution model, and the red dotted line is the lower resolution model using only 100. The agreement between the 10 000 and 1000 cell models show that the shape of the 100 cell model is incorrect due to an insufficient resolution.

forms of ZDI, the rotation phase must be covered as we cannot map the surface of a star without seeing the full surface, nor recover locations of features without good indications of when they rotate in and out of view. In contrast, the pulsation phase does not need to be as well covered in the case where the modes have already been identified, as all we are attempting to fit here is the phase, tangential to radial displacement ratio, and velocity amplitude for each mode. This is simpler than full mode identification.

4.5. Rotation-pulsation period ratio

In some stars the rotation and pulsation frequencies can be very similar, for instance SPBs commonly have both rotation and pulsation periods of the order of 1 c.d–1. If data is taken over a short baseline, at every point in the rotation phase observed, the same point in pulsation phase will be sampled. This makes it difficult to disentangle the pulsations from permanent features. When scheduling observations for such cases, the baseline of observations must be considered. It is best practice to ensure the observations are taken over an entire semester, rather than during a short stint.

4.6. Dependence on the pulsation modes

The higher the number of modes, the more data that is required to fit the pulsation parameters. This is independent of whether or not the modes are identified in advance of the spectropolarimetric observations being taken. Likewise, this is the case for more complex mode geometries, especially when there are multiple pulsation modes present. With fewer observations, and poorer phase coverage, the code is more likely to confuse features from different modes causing significant errors in the brightness and magnetic field mapping. Errors in mode identification can also cause significant issues, though the errors in this case tend to lead to obviously incorrect results, for example extreme bright or dark spots in the brightness map similar to those seen while performing ZDI on pulsating stars with ZDIPY. In some cases, this could mean that the brightness mapping step could help improve mode identification.

4.7. Pulsation amplitudes

If line profile variations due to pulsation are not detectable for a star, it is unlikely that PIMMS is required to map them. Past the detection threshold, it is ultimately a question of the required precision for the desired use. In the case of performing magneto-asteroseismology, we are striving for maximal precision in magnetic field strength and geometry, which requires use of PIMMS. In the case of simply estimating magnetic field strengths and geometries of stars with small pulsation amplitudes, the increased runtime and required pulsation mode identification can be skipped for a reduction in precision.

5. Discussion and conclusions

In this paper we show for the first time that ZDI can be performed accurately on pulsating magnetic stars by including an additional time-dependent velocity map to the fitting procedure. PIMMS will allow us to obtain a more precise characterisation of the magnetic field at the surface of pulsating stars. This will be essential for constraining magneto-asteroseismic models in the future. The upcoming PLATO mission, scheduled to launch in early 2027, will provide long baseline, high cadence photometric data (Rauer et al. 2025). PIMMS will be able to contribute to the ultra-precise stellar characterisations needed both for PLATO exoplanet and stellar evolution research.

The results we obtain with our code PIMMS are subject to the same limits as standard ZDI faces. PIMMS also has a larger data requirement due to the pulsation phases that must be additionally covered and the velocity map that must be fitted. The magnitude of the increase in data is dependent on the number of pulsation modes and their geometries, as well as observing strategies for sampling the rotation and pulsation phases. This makes it hard to predict the number of spectropolarimetric observations needed without first characterising the pulsations.

The model used in this version of PIMMS only considers the effects of pulsation on velocity, while it is known to also affect temperature and brightness. For slowly rotating SPB and β Cep stars, De Ridder et al. (2002) has shown the effect of local temperature variations on the surface-integrated line profiles are negligible. In the case of rapidly rotating stars, the spherically symmetric description of the star and its pulsations breaks down, so the code cannot accurately model such a star's line profile variations regardless. Further work to include the effects of rapid rotation into the stellar models are not currently planned due to the difficulty in detecting their magnetic fields with spectropolarimetry, and the complexity in identifying their pulsation modes.

It is also currently assumed in PIMMS that the line forming region is geometrically thin, such that the local Doppler shift is not dependent on line depth. Zeeman-Doppler imaging is commonly performed on average line profiles calculated using the least-squares deconvolution technique (LSD; Donati et al. 1997), which uses the same assumption, so is consistent. Stellar atmospheres are however stratified by magnetic fields, as they strongly influence diffusion. This could allow us to probe different layers of the stellar atmosphere (Nomura et al. 2012). Incorporating such depth-dependence into the model would require a large number of free parameters, and reduce the S/N of the data as LSD would no longer be possible, hence should be approached with caution and thoroughly tested in the future.

Currently, PIMMS requires that the degree ℓ , azimuthal order m , and frequency f of each pulsation mode is provided a priori, i.e. mode identification must be performed with another method. As it is possible to perform mode identification from the spectropolarimetric data itself, and it is known that magnetic fields affect the allowed pulsation modes, it would therefore be better if the mode identification was performed simultaneously with the magnetic field mapping. Using Doppler shifts to map pulsations has been done previously by Kochukhov (2004), and allows for a more complex description without a parameterisation using a small number of specific spherical harmonics.

The next step is to begin applying PIMMS to real stars. A few magnetic pulsating stars with a sufficient spectropolarimetric data set, and well characterised pulsation modes, have been identified and will be the subject of future papers. In addition, we are currently performing an observing campaign to gain sufficient data for additional magnetic pulsating targets.

Acknowledgements. We thank the anonymous reviewer for their constructive comments, which in particular helped improve the clarity of Sect. 2.3. We are also grateful to Oleg Kochukhov for valuable discussions throughout the development of this software. C.P.F. received funding from the European Union's Horizon Europe research and innovation programme under grant agreement No. 101079231 (EXOHOST), and from the United Kingdom Research and Innovation (UKRI) Horizon Europe Guarantee Scheme (grant number 10051045).

References

- Aerts, C., Christensen-Dalsgaard, J., & Kurtz, D. W. 2010, *Asteroseismology* (Berlin: Springer)
- Briquet, M., Neiner, C., Aerts, C., et al. 2012, *MNRAS*, 427, 483
- Brown, S. F., Donati, J. F., Rees, D. E., & Semel, M. 1991, *A&A*, 250, 463
- Buyschaert, B., Aerts, C., Bowman, D. M., et al. 2018, *A&A*, 616, A148
- Cang, T. Q., Petit, P., Donati, J. F., et al. 2020, *A&A*, 643, A39
- De Ridder, J., Dupret, M. A., Neuforge, C., & Aerts, C. 2002, *A&A*, 385, 572
- Donati, J. F., & Brown, S. F. 1997, *A&A*, 326, 1135
- Donati, J. F., Semel, M., Carter, B. D., Rees, D. E., & Collier Cameron, A. 1997, *MNRAS*, 291, 658
- Donati, J. F., Wade, G. A., Babel, J., et al. 2001, *MNRAS*, 326, 1265
- Donati, J. F., Howarth, I. D., Jardine, M. M., et al. 2006, *MNRAS*, 370, 629
- Finocci, B., & Donati, J. F. 2022, *MNRAS*, 516, 5887
- Folsom, C. P., Bouvier, J., Petit, P., et al. 2018, *MNRAS*, 474, 4956
- Fuller, J., Cantiello, M., Stello, D., Garcia, R. A., & Bildsten, L. 2015, *Science*, 350, 423
- Gray, D. F. 2005, *The Observation and Analysis of Stellar Photospheres* (Cambridge: Cambridge University Press)
- Kochukhov, O. 2004, *A&A*, 423, 613
- Kochukhov, O., & Piskunov, N. 2002, *A&A*, 388, 868
- Kochukhov, O., & Wade, G. A. 2016, *A&A*, 586, A30
- Kochukhov, O., Bagnulo, S., Wade, G. A., et al. 2004, *A&A*, 414, 613
- Kochukhov, O., Mantere, M. J., Hackman, T., & Ilyin, I. 2013, *A&A*, 550, A84
- Kurtz, D. W. 1982, *MNRAS*, 200, 807
- Lecoanet, D., Bowman, D. M., & Van Reeth, T. 2022, *MNRAS*, 512, L16
- Li, G., Deheuvels, S., Ballot, J., & Lignières, F. 2022, *Nature*, 610, 43
- Neiner, C. 2024, <https://zenodo.org/records/13858002>
- Nomura, T., Naito, J., & Shibahashi, H. 2012, *PASJ*, 64, 9
- Rauer, H., Aerts, C., Cabrera, J., et al. 2025, *Exp. Astron.*, 59, 26
- Reed, M. D., Brondel, B. J., & Kawaler, S. D. 2005, *ApJ*, 634, 602
- Rosén, L., & Kochukhov, O. 2012, *A&A*, 548, A8
- Semel, M. 1989, *A&A*, 225, 456
- Shibahashi, H., & Aerts, C. 2000, *ApJ*, 531, L143
- Shultz, M. E., Wade, G. A., Rivinius, T., et al. 2019, *MNRAS*, 490, 274
- Skilling, J., & Bryan, R. K. 1984, *MNRAS*, 211, 111
- Yu, L., Donati, J.-F., Hébrard, E. M., et al. 2017, *MNRAS*, 467, 1342